

## EXTRAGALACTIC SCIENCE WITH TUNABLE FILTERS

Sylvain Veilleux<sup>1</sup>

### RESUMEN

Los filtros sintonizables proporcionan posibilidades únicas para llevar a cabo una amplia gama de proyectos extragalácticos. El énfasis de esta reseña es sobre la ciencia relacionada con los brotes de formación estelar y galaxias activas. También se discuten brevemente futuras rutas de investigación con telescopios de la clase de 8 metros equipados con filtros sintonizables.

### ABSTRACT

Tunable filters provide unique capabilities to carry out a wide array of extragalactic projects. The emphasis of this review is on science relating to starburst and active galaxies. Future avenues of research with 8-meter class telescopes equipped with tunable filters are also discussed briefly.

*Key Words:* **GALAXIES: ACTIVE — GALAXIES: STARBURST — GALAXIES: HIGH-REDSHIFT — INSTRUMENTATION: INTERFEROMETERS — INTERGALACTIC MEDIUM**

### 1. INTRODUCTION

Recent technological developments in the fabrication of high-performance Fabry-Perot etalons<sup>2</sup> have allowed the implementation of reliable and cost-effective tunable filters with wide monochromatic field of view and adjustable transmission characteristics. Deep optical emission-line surveys with a prototype tunable filter on the 3.9m Anglo-Australian Telescope, the Taurus Tunable Filter (or TTF), have shown that there is a rich field of science awaiting exploration with large ground-based telescopes equipped with these narrow-band imagers.

In §2 of this review, I briefly describe the TTF and discuss technical issues relevant to the use of tunable filters in general. In §3, I summarize some of the extragalactic projects conducted with the TTF, emphasizing recent data obtained by our group on starburst and active galaxies. In §4, I discuss possible avenues of research with 8-meter class telescopes equipped with tunable filters. The discussion focusses on the Maryland-Magellan Tunable Filter for the Magellan I 6.5-meter telescope, and comparisons of the capabilities of this instrument with those of OSIRIS on the Grantecan 10.2m telescope.

<sup>1</sup>Department of Astronomy, University of Maryland, USA.

<sup>2</sup>Parallelism between the two highly polished plates of glass in these etalons can be maintained down to spacings of 2  $\mu\text{m}$  (measured at the coating surfaces). Long-range stacked piezoelectric transducers allow the parallel plates to be scanned over a physical spacing of 4  $\mu\text{m}$  (5 wavelengths or 10 interference orders in the I band). Reflective coatings are laid down with ionic bombardment which allows for very high integrity and uniformity in the coating response over a broad wavelength range.

### 2. INSTRUMENTAL TECHNIQUES

All of the observations reported in this review were carried out with the Taurus Tunable Filter (TTF). This instrument has now been decommissioned. It was in operation from 1996 to 2003 on the Anglo-Australian Telescope and 1996 – 1999 on the William Herschel Telescope (WHT; Bland-Hawthorn & Kedziora-Chudczer 2003). Over these years, the TTF was used for several extragalactic surveys; a short summary is given in §3. Developed at the Anglo-Australian Observatory, the TTF design is based on the concept of a conventional Fabry-Perot (FP) interferometer. Using two parallel plates of high reflectivity, light travels through the interferometer such that at each radius from the optical axis a specific wavelength is imaged, resulting in the wavelength,  $\lambda$ , varying linearly with the cosine of the angle from the optical axis,  $\theta$ :

$$m\lambda = 2\mu l \cos\theta, \quad (1)$$

where  $m$  is the order number and  $l$  is the spacing between the two plates. Plate parallelism is maintained down to  $\sim 2 \mu\text{m}$  and scan is possible over a range of  $\sim 10 \mu\text{m}$ . This allows the instrument to work at low orders of interference and thus ensures that the wavelength varies little ( $\lesssim 20 \text{ \AA}$ ) over the full field of view. In other words, it is possible to obtain quasi-monochromatic images with a single exposure. The monochromatic spot is defined as having a radius such that the gradient from center to edge of the spot roughly equals  $\delta\lambda$ , the width of the etalon bandpass. In the case of a Fabry-Perot etalon, the relative change in wavelength  $[\lambda(0) - \lambda(\theta)]/\lambda(0)$  as

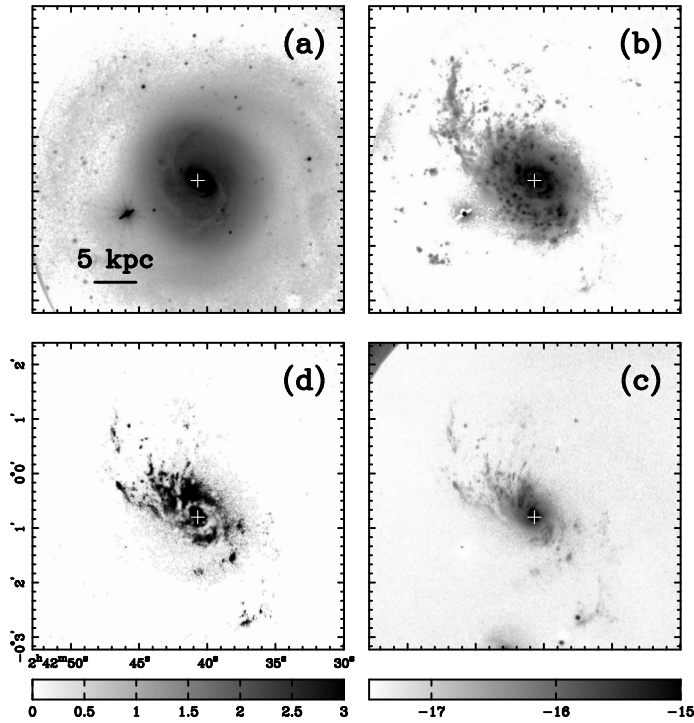


Fig. 1. NGC 1068 in (a) R0 continuum, (b)  $H\alpha$ , (c)  $[\text{O III}] \lambda 5007$ , and (d)  $[\text{O III}] \lambda 5007/H\beta$  ratio ( $\equiv 2.85 \times [\text{O III}] \lambda 5007/H\alpha$ ). North is up and east to the left. The cross in each panel marks the location of the nucleus from NED. The flux scale of the emission-line maps is logarithmic, while the ratio map is on a linear scale. The flux scale for the  $[\text{O III}]$  data ranges from  $-17.5$  to  $-15.0$ , while the scale for the  $H\alpha$  map ranges from  $-18.5$  to  $-15.0$ . Emission from both  $[\text{O III}]$  and  $H\alpha$  is detected for the first time out to  $\sim 11$  kpc from the nucleus in the north-east (upper left) and south-west (lower right) quadrants, roughly aligned with the ionization cone on smaller scale. Note the high  $[\text{O III}]/H\beta$  ratios in the large-scale filaments, indicative of AGN photoionization. The diffuse emission features at the eastern edge of panel (b) and southern edge of panel (c) are artifacts of reflective ghosts associated with the TTF.

a function of off-axis angle  $\theta$  is  $1 - \cos \theta \simeq \theta^2/2$  so

$$\frac{\theta_{\text{mono}}^2}{2} \simeq \frac{\delta\lambda}{\lambda}. \quad (2)$$

For wavelength  $\lambda$ , the bandpass relates directly to the order  $m$  such that  $\delta\lambda = \lambda/R = \lambda/Nm$ , where  $R$  is the spectral resolution and  $N$  is the finesse. Combining this expression with Eqn. (2) we find that the angle subtended by the monochromatic spot is

$$\theta_{\text{mono}}^2 \simeq 2/Nm = 1/(20 \times m). \quad (3)$$

For a particular etalon (e.g.,  $N = 40$ ), the size of the monochromatic spot depends on order  $m$  alone. Eqn. (3) shows how the spot covers increasingly larger areas on the detector as the filter is used at lower orders of interference.

The bandwidth of the TTF was adjustable from  $\sim 6$  to  $60 \text{ \AA}$ , thus making it possible to obtain very narrow-band images. For instance, it has been used to separate the  $H\alpha$  and  $[\text{N II}] \lambda 6583$  emission lines, a

difficult task with conventional narrow-band filters. The wavelength coverage of the TTF was from  $3700 \text{ \AA}$  to  $6500 \text{ \AA}$  (Blue TTF) and from  $6000 \text{ \AA}$  to  $9500 \text{ \AA}$  (Red TTF).

The TTF at the AAT also had the ability to switch between frequencies at a very rapid rate, up to  $\sim 100$  Hz if needed, although in most cases, the charges were moved only every 1-2 minutes and the chip was read after typically spending 32 minutes of integration time (16 minutes on-band and 16 minutes off-band). By shuffling the charge of the CCD in sync with the frequency switching, an object could be observed at two distinct frequencies (and two distinct bandwidths) *at almost the same time*. This technique helps average out temporal effects associated with atmospheric and instrumental variations and improves the spectrophotometric accuracy and sensitivity to faint emission-line sources:  $\sim a \text{ few} \times 10^{-18} \text{ erg s}^{-1} \text{ cm}^{-2} \text{ arcsec}^{-2}$  or about 10x better than typical narrow-band images. The TTF on the AAT was

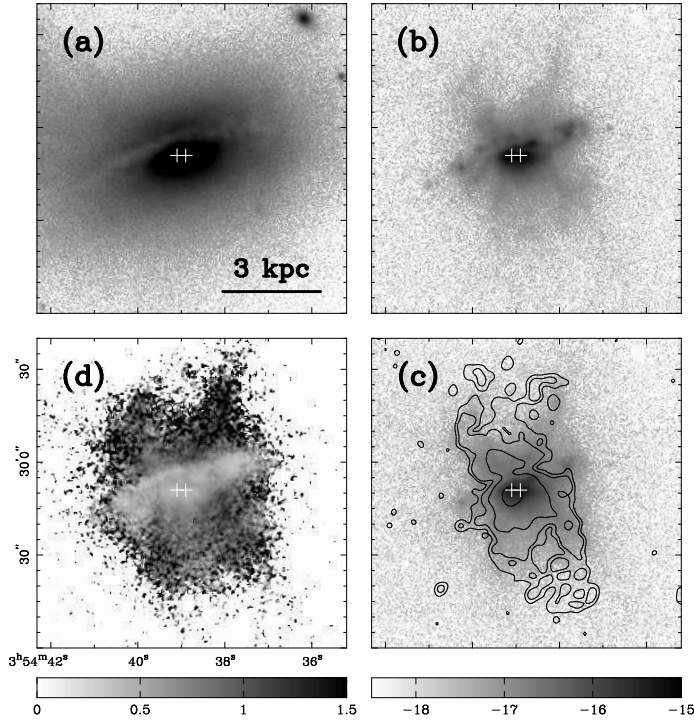


Fig. 2. Galactic wind in NGC 1482: (a) R0 continuum, (b)  $H\alpha$ , (c)  $[N II] \lambda 6583$  and *Chandra* X-ray contour map, and (d)  $[N II] \lambda 6583/H\alpha$  ratio. North is up and east to the left. The crosses in each panel indicate the locations of the two peaks in the red continuum. The flux scale of the emission-line maps is logarithmic, while the ratio map is on a linear scale. The contour levels of the X-ray map are at  $3.0, 5.4, 17,$  and  $169 \times 10^{-4}$  counts  $s^{-1}$  arcsecond $^{-2}$  (based on an effective exposure time of 24.40 ksec). Note the tight match between the X-ray emission and some of the optical filaments.

often used in a straddle mode, where the off-band image is made up of a pair of images that “straddle” the on-band image in wavelength (e.g.,  $\lambda_1 = 6500 \text{ \AA}$  and  $\lambda_2 = 6625 \text{ \AA}$  for rest-frame  $H\alpha$ ); this greatly improves the accuracy of the continuum removal since it corrects for slopes in the continuum and underlying absorption features. The charge shuffling and frequency switching capabilities were not available at the WHT.

For more detail on the TTF, the reader should refer to Bland-Hawthorn & Jones (1998) and Bland-Hawthorn & Kedziora-Chudczer (2003). Several papers have been published on the data acquisition and reduction techniques used to reach low flux levels with the TTF (see, e.g., Shopbell et al. 1999; Glazebrook & Bland-Hawthorn 2001; Veilleux & Rupke 2002; Jones, Shopbell, & Bland-Hawthorn 2002; Miller & Veilleux 2003a).

### 3. EXTRAGALACTIC SCIENCE

#### 3.1. Overview

The TTF has been used for a wide variety of extragalactic projects. Here are some examples:

- Local galaxies: inactive edge-on spirals (Miller & Veilleux 2003a), face-on spirals (Cianci 2003a,b), ellipticals (Ferguson et al. 2001; Ryder, Fenner, & Gibson 2002), starbursts (Veilleux et al. 2003), and active galaxies (Shopbell et al. 1999; Tadhunter et al. 2000; Solorzano-Inarrea et al. 2002; Veilleux & Rupke 2002; Solorzano-Inarrea & Tadhunter 2003; Veilleux et al. 2003).
- Galaxies clusters: cooling flows (Jaffe & Bremer 2000; Edge et al. in prep.); intra-cluster planetary nebulae (Arnaboldi et al. 2003); effect of possible EUV intra-cluster emission on gas-rich spirals (Maloney & Bland-Hawthorn 2001).
- Emission-line galaxy surveys: field galaxies (Jones & Bland-Hawthorn 2001; Tober et al. 2004, submitted); clusters (Zaritsky & Jones in prep.); quasar environment (Baker et al. 2001); quasar sight lines (Francis et al. 2001a, 2001b).

The results from these surveys were nicely summarized in Bland-Hawthorn & Kedziora-Chudczer

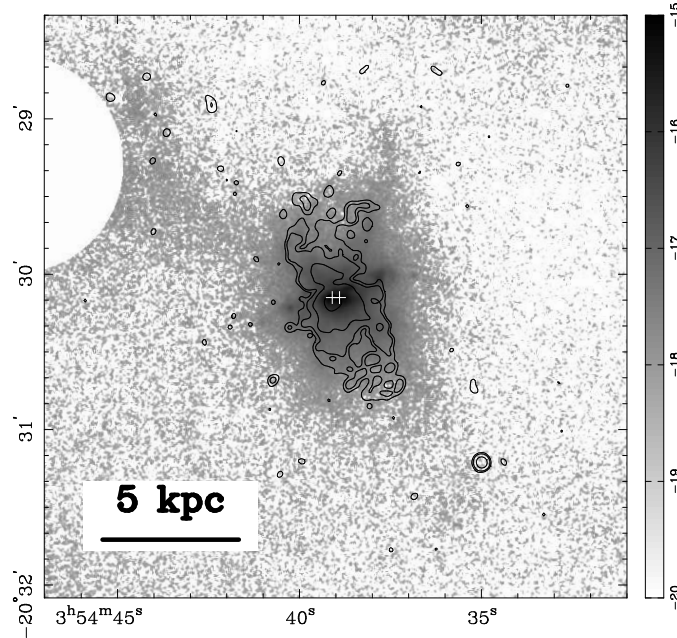


Fig. 3. *Chandra* X-ray contour map superposed on a very deep  $H\alpha + [N II] \lambda 6583$  image of NGC 1482. North is up and east to the left. The crosses indicate the locations of the two peaks in the red continuum. The flux scale is logarithmic. The contour levels of the X-ray map are the same as in Figure 2. Filamentary line emission is detected out to  $\sim 7$  kpc north-west of the nucleus, and perhaps out to  $\sim 12$  kpc to the north-east. Diffuse emission may also be present  $\sim 10$  kpc south of the nucleus. A bright star on the eastern edge of the image was masked for display purposes; it may be responsible for reflective ghosts that can be confused with faint emission-line features.

(2003); this discussion will not be repeated here. The remainder of this section focusses on a TTF survey of nearby galaxies recently completed by our group.

### 3.2. Warm Ionized Gas in Normal, Starburst, and Active Galaxies

Our group has used the TTF on the AAT and WHT to map several active and starburst galaxies as well as a number of normal (“quiescent”) edge-on disk systems. The portion of the survey on normal galaxies was part of a Ph.D. thesis by University of Maryland student Scott T. Miller. The main goals of this survey were to search for warm ( $T \approx 10^4$  K) line-emitting gas on the outskirts of these galaxies, and study the properties of this gas to constrain its origin and overall importance. The starburst and active galaxies were selected based on the fact that they all present ionization cones and/or galactic winds on  $\sim$  kpc scale. The normal galaxies are all edge-on disk galaxies with an inclination larger than  $\sim 80^\circ$  (often  $i > 85^\circ$ ). This was done to facilitate separation of the disk emission from that of the halo.

The results of this survey can be summarized as follows (Miller & Veilleux 2003a, 2003b; Veilleux et al. 2003; see Figs. 1 – 5):

- In active and starburst galaxies, ionized filaments are often seen extending out to several tens of kpc, sometimes beyond the H I edge of the host galaxy. The topology and projected cross-section of the line-emitting gas varies widely among the galaxies in the sample. Very large ( $\gtrsim 80$  kpc) ionized complexes are discovered around NGC 6240 (Fig. 4) and MR 2251–178 (Fig. 5). Emission-line knots and wispy filaments are confirmed to be present in the halo of NGC 4388 at distances of up to  $\sim 30$  kpc from the active nucleus. Diffuse and filamentary gas associated with large-scale (10 – 20 kpc) ionization cones or outflows are detected for the first time in NGC 1068 (Fig. 1), NGC 1365, and NGC 1482 (Figs. 2 – 3) and confirmed in NGC 7213. Emission-line structures on  $\gtrsim$  kpc scale are revealed in the galactic winds of NGC 1705, Circinus galaxy, and ESO484-G036.
- Filamentary complexes are seen extending a few kpc above and below the disks of normal star-forming galaxies. Both the mass and extent of the extraplanar material in these galaxies ap-

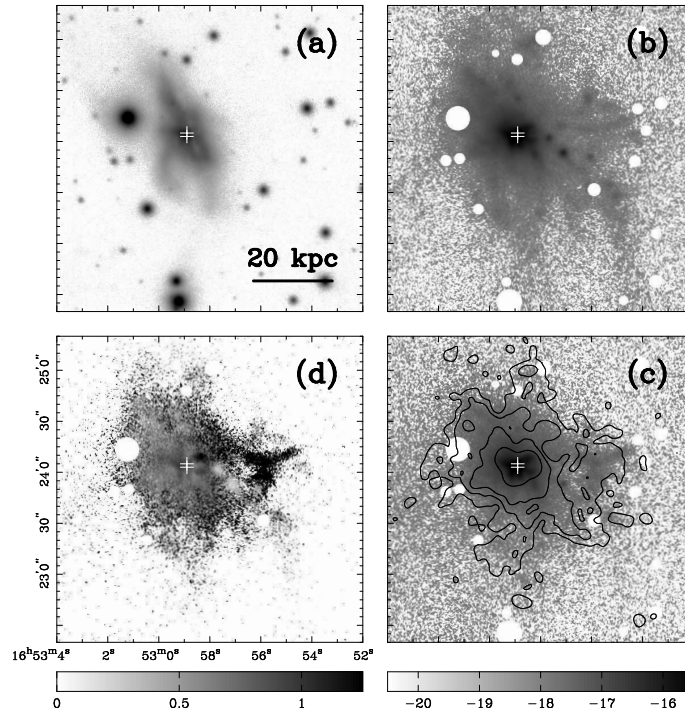


Fig. 4. Outer regions of NGC 6240 in (a) R0 continuum, (b)  $H\alpha$ , (c)  $[N II] \lambda 6583$  and *Chandra* X-ray contour map from Komossa et al. (2003), and (d)  $[N II] \lambda 6583/H\alpha$  ratio. North is up and east to the left. The crosses indicate the positions of the binary AGN in this object. The flux scale of the emission-line maps is logarithmic, while the ratio map is on a linear scale. The contour levels of the X-ray map are at  $7.0, 14, 28,$  and  $111 \times 10^{-4}$  counts  $s^{-1} \text{arcsec}^{-2}$  (based on an effective exposure time of 37 ksec). Complex filamentary emission extends over  $70 \times 80$  kpc. Note the good match between the X-ray emission and the high- $[N II]/H\alpha$  loop and filament at  $R \approx 15 - 25$  kpc and P.A.  $\approx 270^\circ$ . These features are probably associated with a galactic outflow.

pear to be correlated with the *local* surface density of star formation activity in the disk.

- Emission-line ratio maps constructed from multi-line imaging of these objects reveal line ratios which are not H II region-like. A detailed analysis of our results on normal disk galaxies suggests that the extraplanar material is ionized by a secondary source of ionization in addition to photoionization by the OB stars in the disk (Miller & Veilleux 2003b). In active galaxies, the primary source of ionization of the extended nebula is either the AGN itself or shock excitation associated with a large-scale outflow.
- Multi-line imaging slightly shifted in velocity space provides strong constraints on the kinematics of the warm ionized gas. In all cases studied so far, the gas appears to be bound to the host galaxy.

Given the small size of the sample and the methods of selection of the sample, no statistical state-

ment can be made on the frequency of occurrence of large-scale nebulae around starburst and active galaxies in general (recall that the objects in our sample were specifically selected to host ionization cones and/or galactic winds on  $\sim$  kpc scale). The high discovery rate of  $\gtrsim 10$ -kpc nebulae in our sample may not be typical of the local population of starburst and active galaxies. The advent of tunable filters on 8-meter class telescopes should improve the sensitivity of emission-line galaxy surveys at least tenfold and allow us to expand the sample to a more representative set of objects.

#### 4. FUTURE: MMTF AND OSIRIS

Within a year or two, “clones” of the TTF will be commissioned on 8-meter class telescopes. OSIRIS (e.g., Cepa this conference) will be available on the GTC, the Maryland-Magellan Tunable Filter (MMTF) will be available on the 6.5m Magellan I telescope, and the Prime Focus Imaging Spectrograph (PFIS) for the South African Large Telescope (SALT) will be equipped with a tunable filter. In this

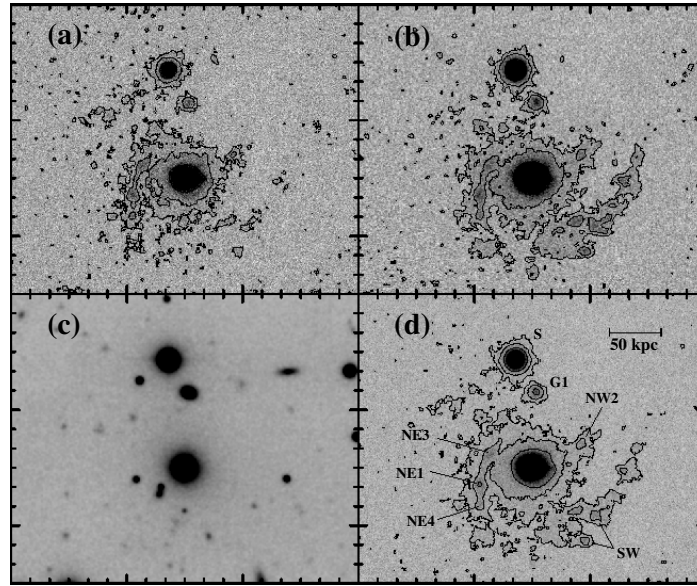


Fig. 5. Deep H $\alpha$  and I-band images of the field surrounding the quasar MR 2251-178, reproduced from Shopbell, Veilleux, & Bland-Hawthorn (1999). Panels (a) and (b) are 1200-second exposures at redshifts of 0.0640 and 0.0645, respectively, panel (c) is an I-band continuum image of the same field, and panel (d) is a summed H $\alpha$  image. North is up and east to the left. The flux scale is logarithmic. A bright star (S), a nearby cluster galaxy (G1), and a number of emission-line knots from Macchetto et al. (1990) have been labeled. The emission is detected on a scale of  $\sim 200$  kpc.

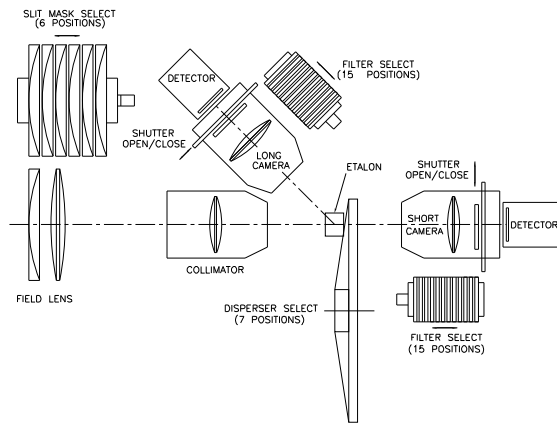


Fig. 6. Design of IMACS. The tunable filter will be inserted in the disperser system server and used with the short camera. The blocking filters will be inserted in the filter server associated with this camera.

section, I first describe the MMTF and then make comparisons between the MMTF and OSIRIS.

#### 4.1. *The Maryland-Magellan Tunable Filter (MMTF)*

The MMTF is a NSF-funded collaboration between the University of Maryland, Carnegie, and AAO; the PI for this project is the author.

**IMACS.** The MMTF will be mounted in IMACS<sup>3</sup>, the Inamori Magellan Areal Camera and Spectrograph. IMACS mounts at the Nasmyth focus of Magellan I. Fed by the f/11 Gregorian configuration, with an integral atmospheric dispersion corrector (ADC) and field corrector mounted at the tertiary mirror, the transmitting, all-spherical collimator produces a well corrected, unvignetted field of 24' in diameter, and slightly vignetted field of 30' in diameter. As shown in Figure 6, two cameras are used to re-image the 150-mm diameter collimator exit pupil at 0''.111 and 0''.200 pixel<sup>-1</sup>. To avoid any major modifications to the design of IMACS and optimize the field of view, the tunable filter will strictly utilize the short focal length camera (0''.2 pixel<sup>-1</sup>). The CCD array in IMACS consists of a mosaic of 8 SITE ST-002A 2048  $\times$  4096 devices with 15  $\mu$ m pixels.

**The Tunable Filter in IMACS.** The MMTF will have characteristics that resemble those of the “red” TTF on the AAT. The etalon is from IC Optical Systems Ltd (formerly Queensgate Instruments). This company has a long history of manufacturing high-quality etalons for astronomers, including the low-order etalons for the TTF. An ET150 etalon with

<sup>3</sup>The IMACS project homepage is <http://www.ociw.edu/instrumentation/imacs/>.

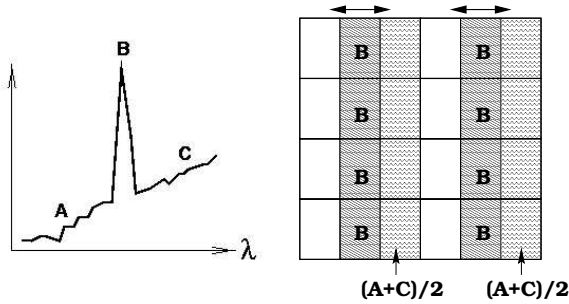


Fig. 7. Charge shuffling with the tunable filter and IMACS CCD  $2 \times 4$  array. The charge on the chip are shuffled left and right at the same rate that the etalon plates are scanned between two discrete gap positions. The chip is read only once. The central third of each CCD is used for the on-band image. The off-band image is on the right of each on-band image while the left third of each CCD is used for charge shuffling purposes only. In the case shown here the off-band image “straddles” the on-band band image in wavelength. This adaptive frequency switching improves continuum subtraction and can also be used to avoid OH sky lines.

150-mm open aperture is the etalon of choice to avoid significant vignetting of the IMACS beam. The wavelength coverage will be approximately  $5000 - 9200 \text{ \AA}$ . The finesse of the etalon will be  $\sim 40$ .

The tunable filter will be installed in the 150-mm collimated beam of IMACS in one of six interchangeable positions of the disperser server. Assuming  $m = 2 - 15$  for the MMTF (the same as TTF), eqn. (3) implies  $\theta_{\text{mono}} = 9^\circ - 3^\circ$ . The monochromatic spot of the MMTF therefore still covers about  $1/3$  of the FOV or  $\sim 10'$  in the worst case scenario (highest resolution, highest  $m$ ).

The 20-kg CS100 unit which controls and monitors the piezo-electric transducers and capacitance micrometers on the etalon will be installed in the electronic rack on the Nasmyth platform. The cabling between the etalon, the disperser server and the CS100 controller will be broken at each of several bulkheads with connectors and feed-throughs (already in place).

#### Charge Shuffling and Frequency Switching.

Two basic modes of operation will be available on the tunable filter. The first is standard narrowband imaging where the available field of view is the whole  $27' \times 27'$  of the short camera. The second mode makes use of charge shuffling and frequency switching. The idea will be to move the charge left and right within each of the eight detectors in IMACS at the same time as switching between two discrete frequencies with the tunable filter (see Fig. 7). The

switching rate ( $< 1 \text{ Hz}$ ) will be limited by the shutter rather than by charge transfer efficiency of the CCDs. Charge shuffling will be done by inserting a slit mask at the focal surface of the telescope, with two long rectangles, each corresponding to  $1/3$  of the width of a 4K detector, or  $27'/6 = 4.5'$  wide. Then two blocks of pixels, each  $1/3$  of 4K long, can be alternately shuffled into the viewing region. This gives  $\sim 250$  square-arcminutes of non-contiguous viewing area (equivalent area to a  $15.6' \times 15.6'$  square). To produce a contiguous field of view, one will nod the telescope twice by  $\pm 4.5'$  between each CCD readout. A “straddle” option will also be available in this charge shuffling mode (see §2).

#### 4.2. Expected Performances of the MMTF and OSIRIS

The MMTF will combine the wide-field monochromatic imaging capabilities of the TTF with the large aperture and superb delivered image quality (median seeing  $\sim 0.6''$ ) of Magellan I, and the excellent photometric characteristics of the Las Campanas site. The expected performance of the MMTF can be estimated from the current capabilities of the TTF and the expected characteristics of IMACS. The overall efficiency of IMACS in the imaging mode reaches a value of  $\sim 70\%$  at  $7000 \text{ \AA}$  and remains  $\gtrsim 40\%$  over the range  $4000 - 9500 \text{ \AA}$ . This is similar to the Taurus system on the AAT (without the etalon and blocking filter). Assuming similar etalon and blocking filter efficiencies for the TTF and MMTF systems, the relative sensitivity of these systems to emission-line point sources then scales with the squared telescope apertures ( $6.5\text{m}$  vs.  $3.9\text{m}$ ) and inverse squared FWHMs of the delivered images ( $0.6''$  vs.  $1.2''$ ), resulting in a gain of an order of magnitude in sensitivity for the MMTF relative to the TTF. Point sources with emission-line fluxes of a few  $\times 10^{-18} \text{ erg s}^{-1} \text{ cm}^{-2}$  within the  $27'$  FOV of the MMTF should be detectable ( $3 \sigma$ ) in an hour or less, depending on wavelength. The MMTF will be well suited to search for emission-line galaxies at  $z \lesssim 6.5$  (Fig. 8). Commissioning of the MMTF is scheduled for fall 2004. This instrument should be available to the Magellan community starting in semester 05A or 05B.

The capabilities of the MMTF will in many ways complement those of the OSIRIS tunable filters on the GTC. Given the larger diameter of the GTC, the sensitivity to point sources of OSIRIS should be 2-3 times better than that of the MMTF, assuming everything else is the same (e.g., throughput, delivered image quality). The large FOV of the MMTF will be

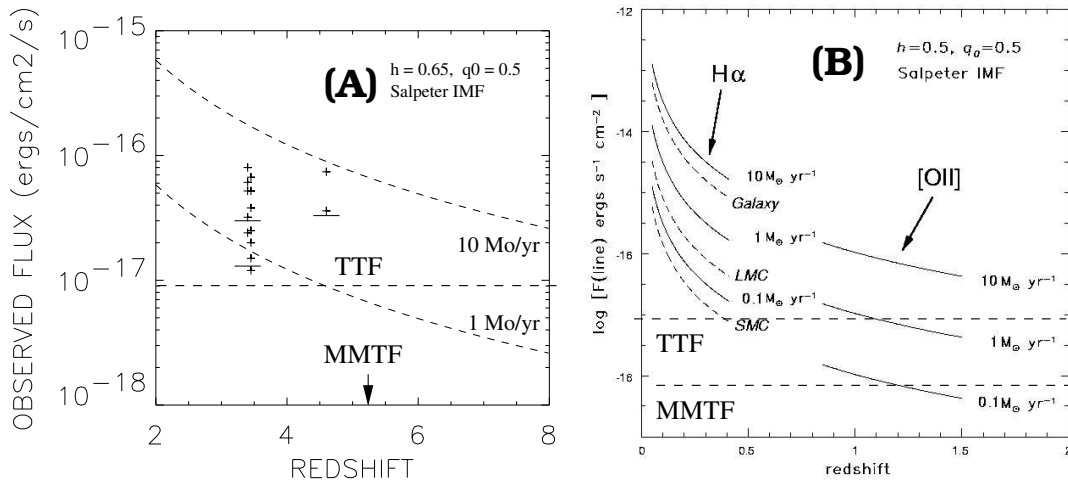


Fig. 8. (a) Ly $\alpha$  line fluxes for galaxies with SFR = 1 or 10 M<sub>⊙</sub> yr<sup>-1</sup> as a function of redshift. This assumes a Kennicutt (1983) relation between H $\alpha$  luminosity and star formation rate, and a ratio of Ly $\alpha$  to H $\alpha$  (8.7) that applies for Case B recombination (*i.e.* no extinction). Crosses show the Ly $\alpha$  fluxes of the objects in the Hawaii surveys (see Hu 1998 and references therein). (b) Unobscured H $\alpha$  (*left*) and [OII] line fluxes (*right*) for galaxies with SFR = 0.1 – 10 M<sub>⊙</sub> yr<sup>-1</sup> as a function of redshift. Star-formation rates for the Galaxy (5 M<sub>⊙</sub> yr<sup>-1</sup>), the LMC (0.26 M<sub>⊙</sub> yr<sup>-1</sup>), and SMC (0.046 M<sub>⊙</sub> yr<sup>-1</sup>) are shown for comparison. Adapted from Bland-Hawthorn et al. (2001).

best suited for wide-area surveys, while OSIRIS will be able to search for fainter sources. OSIRIS and MMTF will be an extremely powerful combination to study the line-emitting universe for many years to come.

The TTF survey described in this article was done in collaboration with D. Rupke, P. L. Shopbell, J. Bland-Hawthorn, and G. Cecil. Some of this work was carried out while on sabbatical at the California Institute of Technology and the Observatories of the Carnegie Institution of Washington; the author thanks both of these institutions for their hospitality. The author acknowledges partial support of this research by a Cottrell Scholarship awarded by the Research Corporation, NASA/LTSA grant NAG 56547, and NSF/CAREER grant AST-9874973, as well as NSF/ATI grant AST-0242860 for the commissioning of the MMTF.

#### REFERENCES

Arnaboldi, M., et al. 2003, *AJ*, 125, 514  
 Baker, J. C., et al. 2001, *AJ*, 121, 1821  
 Bland-Hawthorn, J., & Jones, D. H. 1998, *SPIE*, 335, 855  
 Bland-Hawthorn, J. & Kedziora-Chudczer, L. 2003, *PASA*, 20, 242  
 Bland-Hawthorn, J., et al. 2001, *ApJ*, 563, 611  
 Cianci, S. 2003a, *AAO Newsletter*, 102, 4

Cianci, S. 2003b, Ph. D. thesis, University of Sydney  
 Ferguson, A., van der Hulst, T., & van Gorkom, J. 2001, *AAO Newsletter*, 96, 4  
 Francis, P., Wilson, G. M., & Woodgate, B. E. 2001a, *PASA*, 18, 64  
 Francis, P., et al. 2001b, *ApJ*, 554, 1001  
 Glazebrook, K., & Bland-Hawthorn, J. 2001, *PASP*, 113, 197  
 Hu, E. M. 1998, *ASP Conf. Ser.* 146, 148 (*astro-ph/9801170*)  
 Jaffe, W., & Bremer, M. 2000, *AAO Newsletter*, 93, 3  
 Jones, H., & Bland-Hawthorn, J. 2001, *ApJ*, 550, 593  
 Jones, D. H., Shopbell, P. L., & Bland-Hawthorn, J. 2002, *MNRAS*, 329, 759  
 Kennicutt, R. C. 1983, *ApJ*, 272, 54  
 Komossa, St., et al. 2003, *ApJ*, 582, L15  
 Maloney, P. R., & Bland-Hawthorn, J. 2001, *ApJ*, 553, L129  
 Miller, S. T., & Veilleux, S. 2003a, *ApJS*, 148, 383  
 —. 2003b, *ApJ*, 592, 79  
 Ryder, S., Fenner, Y., & Gibson, B. K. 2003, *AAO Newsletter*, 102, 6  
 Shopbell, P. L., Veilleux, S., & Bland-Hawthorn, J. 1999, *ApJ*, 524, 83  
 Solorzano-Inarrea, C., et al. 2002, *MNRAS*, 331, 673  
 Solorzano-Inarrea, C., & Tadhunter, C. N. 2003, *MNRAS*, accepted (*astro-ph/0301157*)  
 Tadhunter, C. N., et al. 2000, *MNRAS*, 314, 849  
 Veilleux, S., & Rupke, D. S. 2002, *ApJ*, 565, L63  
 Veilleux, S., Shopbell, P. L., Rupke, D. S., Bland-Hawthorn, J., & Cecil, G. 2003, *AJ*, 126, 2185

Sylvain Veilleux: Department of Astronomy, University of Maryland, College Park, MD 20742, USA.